Nanoscale

PAPER

View Article Online
View Journal | View Issue

Cite this: *Nanoscale*, 2026, **18**, 4111

From chain to framework: atomically precise silver cluster-assembled architectures

Xiaolin Liu,†[a,b] Taeyoung Ki,†[a,b] Seungwoo Yoo,[a,b] Guocheng Deng, *[a,b] Megalamane S. Bootharaju*[a,b,c] and Taeghwan Hyeon *[a,b]

The controlled assembly of atomically defined metal nanoclusters (NCs) into extended frameworks represents a powerful approach to developing functional materials with tailored properties. However, achieving structural dimensionality (1D–3D) control while maintaining the integrity of a single cluster core remains a significant challenge. Herein, we report the construction of a series of silver cluster-assembled materials (SCAMs) using Ag_{12} clusters and directional N-donor ligands of varying lengths. The resulting architectures—1D $[Ag_{12}(S^tBu)_6(CF_3COO)_6(Py_2S)_2(CH_3CN)_2]$, 2D $[Ag_{12}(S^tBu)_6(CF_3COO)_6(bpm)_3]$, and 3D $[Ag_{12}(S^tBu)_6(CF_3COO)_6(tmdp)_3]$—feature preserved cuboctahedral Ag_{12} cores connected through directional Ag-N bonding. Single-crystal X-ray diffraction confirms structural fidelity across all dimensions. These assemblies provide a rare platform to systematically explore the impact of dimensionality on function. Catalytic tests reveal that all three SCAMs efficiently catalyze the hydrogenation of nitroaromatics to aminoaromatics, with the 1D SCAM exhibiting the highest activity. This work highlights a rational, ligand-directed strategy for creating dimensionally tunable, atomically precise cluster-based frameworks and establishes a direct link between structural dimensionality and catalytic performance. Our findings offer a blueprint for designing next-generation nanomaterials with customized architectures and functions for advanced catalytic and optoelectronic applications.

Received 7th November 2025,
Accepted 21st January 2026

DOI: 10.1039/d5nr04708k

rsc.li/nanoscale

1 Introduction

The colloidal synthesis and self-assembly of nanoparticles have become central themes in nanoscience and materials chemistry, enabling the creation of complex, functional nanomaterials from simple nanoscale units.[1–3] By mimicking nature's design principles—exemplified by the organized structures of DNA and proteins—these assemblies not only offer insights into the origin of life but also open up transformative opportunities in materials design, sensing, catalysis, and electronics.[4–14] Among the diverse nanoparticle types, metal nanoparticles, especially those composed of noble metals, are particularly attractive due to their unique optoelectronic and catalytic properties.[15–18] However, their intrinsic instability and size heterogeneity often hinder precision control over structure–property relationships.

To overcome these challenges, atomically precise metal NCs—small groups of metal atoms protected by organic ligands—have emerged as ideal building blocks. Typically, 1–3 nm in diameter, these clusters exhibit well-defined geometries, quantized electronic structures, and tunable surface chemistry.[19–21] Importantly, the choice and arrangement of ligands not only stabilize the metal core but also play a pivotal role in directing self-assembly, modulating physicochemical properties, and tailoring interactions with the environment.[22–26] Among various metal NCs, Ag NCs are particularly promising due to their strong light–matter interactions, high surface reactivity, and low-cost relative to gold.[27–33] However, Ag NCs are also notoriously sensitive to oxidation and ligand exchange, making them less stable and harder to work with.[34] A promising strategy to address these limitations involves assembling discrete Ag NCs into extended frameworks—known as SCAMs.[35] These architectures retain the atomically precise nature of the building blocks while enhancing stability, enabling new functions *via* collective behavior and extended connectivity.[36–39]

Despite the growing success in constructing SCAMs, controlling the dimensionality (1D, 2D, 3D) of such frameworks from a single type of Ag NCs while preserving its core integrity remains a formidable challenge.[40] Small changes in ligand identity or assembly conditions often lead to core rearrangements, decomposition, or entirely different cluster struc-

[a]*Center for Nanoparticle Research, Institute for Basic Science (IBS), Seoul 08826, Republic of Korea. E-mail: gcdeng@snu.ac.kr, msbootharaju@snu.ac.kr, thyeon@snu.ac.kr*
[b]*School of Chemical and Biological Engineering, and Institute of Chemical Processes, Seoul National University, Seoul 08826, Republic of Korea*
[c]*Centre for Nano and Soft Matter Sciences (CeNS), Shivanapura, Bengaluru 562162, India*
†These authors contributed equally to this work.

tures.[41] Previous reports have demonstrated dimensional transformation from 0D to higher-dimensional architectures using Ag NCs, but these transformations often compromise core geometry and atomic composition.[42,43] As a result, direct comparisons of structure–function relationships across dimensionalities remain elusive.

In this work, we address this critical gap by designing a series of directional N-donor ligands of varying lengths to assemble a single Ag NC, Ag_{12}, into 1D, 2D, and 3D frameworks—while retaining the atomic structure of the metallic core across all architectures. The resulting SCAMs—$[Ag_{12}(S^tBu)_6(CF_3COO)_6(Py_2S)_2(CH_3CN)_2]$ (denoted as **1D Ag_{12}-Py_2S**; Py_2S: 4,4′-dipyridyl sulfide), $[Ag_{12}(S^tBu)_6(CF_3COO)_6(bpm)_3]$ (denoted as **2D Ag_{12}-bpm**; bpm: 3,3′-bipyridine), and $[Ag_{12}(S^tBu)_6(CF_3COO)_6(tmdp)_3]$ (denoted as **3D Ag_{12}-tmdp**; tmdp: 4,4′-trimethylene dipyridine)—feature cuboctahedral Ag_{12} cluster nodes and are connected *via* directional covalent bonding. Single-crystal X-ray diffraction (SCXRD) confirms that the metal cores and ligand shells remain intact, offering a unique platform for systematically studying the effect of dimensionality on material properties. Notably, all three SCAMs exhibit catalytic activity in the hydrogenation of nitrophenol to aminophenol, with the **1D Ag_{12}-Py_2S** structure outperforming its higher-dimensional counterparts. This enhanced activity is attributed to the higher accessibility of catalytically active silver sites in the lower-dimensional framework. These findings not only demonstrate the feasibility of dimensionally tunable, atomically precise Ag cluster frameworks but also underscore the crucial role of structural dimensionality in governing catalytic performance. This work pioneers a rational design strategy for assembling identical metal nanoclusters into tunable dimensional architectures, opening new avenues in the development of precision nanomaterials for catalysis and beyond.

2 Results and discussion

During the assembly process, it remains difficult to design structurally controllable atomically precise materials due to the challenge of preserving the size, structure, and composition of the metal clusters.[41–43] The key lies in selecting both suitable cluster nodes and linkers that can guide the dimensionality of the resulting architectures without disrupting the cluster's integrity. Given the high reactivity and structural flexibility of Ag NCs, achieving predictable and controlled assembly is particularly complex. To address this, we systematically screened a variety of N-donor linkers with different carbon chain lengths and binding motifs to find the right combination of coordination flexibility and structural directionality. Through systematic investigation, we identified the Ag_{12} NC as an ideal building block for dimensional control.[44] As shown in Fig. 1a, the 12 silver atoms in the Ag_{12} NC adopt a cuboctahedral geometry, which can be viewed as a hexagonal plane sandwiched between two triangular planes. Each square face of the cuboctahedron is coordinated with a *tert*-butylthiolate ligand, resulting in a total of six thiolate ligands on the NCs surface

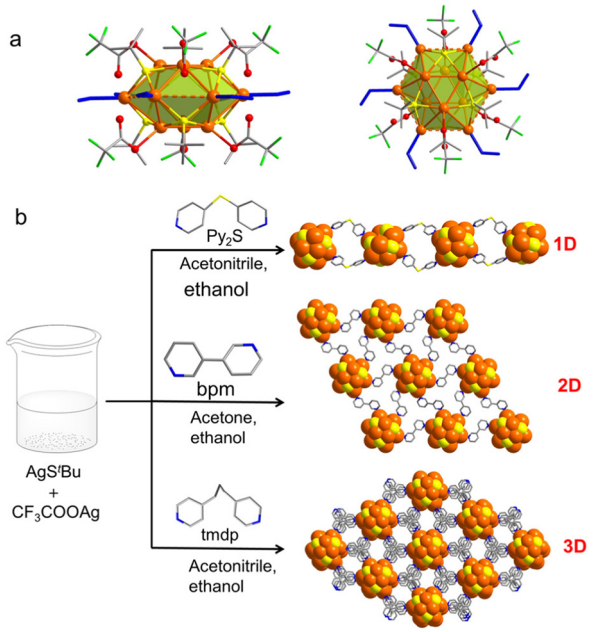

Fig. 1 (a) Side (left) and top (right) views of the Ag_{12} building block. (b) Schematic illustration of the synthesis of 1D, 2D and 3D Ag_{12} cluster-based frameworks. Color legend: orange, Ag; yellow, S; red, O; green, F; blue, N; gray, C. All hydrogen atoms are omitted for clarity.

(Fig. S1a). Additionally, each silver atom located on the top and bottom triangular planes is capped by a trifluoroacetate ion (Fig. S1b), contributing another six ligands. This coordination environment assigns all silver atoms a formal oxidation state of +1. Importantly, the six equatorial silver atoms on the hexagonal plane remain accessible for linker coordination, enabling the programmable assembly of extended architectures (Fig. 1a, blue lines). Through judicious selection of N-donor bidentate linkers (Py_2S, bpm, and tmdp), we successfully constructed dimensionally controlled SCAMs: **1D Ag_{12}-Py_2S**, **2D Ag_{12}-bpm**, and **3D Ag_{12}-tmdp** assemblies, respectively. The intercluster distance and dimensionality are largely determined by the length and flexibility of the linkers. Linear and rigid linkers, such as bpm, are generally favorable for the formation of 2D assemblies, as their planar and linear geometry promotes lateral extension within a plane. Compared with linear bpm, Py_2S is also essentially planar; however, it contains a pronounced bending angle (~100°) at the C–S–C unit, which is unfavorable for 2D propagation but instead promotes the formation of 1D assemblies. In contrast to both bpm and Py_2S, tmdp exhibits greater conformational freedom owing to the presence of a –C–C–C– spacer between the two pyridyl groups, thereby preferentially promoting the construction of 3D frameworks.

These architectures were synthesized *via* a versatile one-pot approach by systematically varying both solvent systems and bridging ligands (Fig. 1b). For the synthesis of **1D Ag_{12}-Py_2S**, equimolar amounts of silver thiolate precursor (AgS^tBu) and silver trifluoroacetate (CF_3COOAg) were added to a 1 : 1 (v/v) solvent mixture of acetonitrile and ethanol (see SI for more

details). The Py_2S linker was subsequently introduced, and the reaction mixture was stirred for 1 hour before filtration. The resulting filtrate was then allowed to evaporate slowly at room temperature, yielding rod-shaped, colorless crystals (Fig. S2) after one week. Following a similar protocol, **2D Ag_{12}-bpm** was synthesized using bpm as the linker in a mixed solvent system of acetone and ethanol, resulting in plate-shaped crystals (Fig. S3). For **3D Ag_{12}-tmdp**, the reaction was carried out in acetonitrile and ethanol with tmdp as the linker, affording block-shaped crystals (Fig. S4). These results highlight how linker selection and solvent conditions play a decisive role in steering the dimensionality of SCAMs, while maintaining the structural integrity of the Ag_{12} building block.

SCXRD analysis reveals that **1D Ag_{12}-Py_2S** crystallizes in the monoclinic $C2/c$ space group (Table S1). Its Ag_{12} cluster building blocks retain a cuboctahedral structure (Fig. 2a). The Ag–Ag bond lengths within the cuboctahedron range from 2.861 to 3.409 Å, with an average of 3.141 Å. Six thiolate ligands are coordinated to the square face of the Ag_{12} cuboctahedron, with Ag–S bond lengths ranging from 2.426 to 2.576 Å and an average of 2.504 Å. Two of the six equatorial silver atoms in the cuboctahedron are each coordinated by one acetonitrile molecule, while the remaining four are bonded through their nitrogen atoms to one end of the bidentate Py_2S linkers. The other end of each linker connects to neighboring Ag_{12} units, resulting in the formation of a one-dimensional chain structure (Fig. 2b). The Ag–N bond distances ranging from 2.297 to 2.314 Å, with an average of 2.306 Å. Six trifluoroacetate ligands are coordinated to silver atoms, with Ag–O bond lengths ranging from 2.362 to 2.532 Å and an average value of 2.418 Å. Among them, two trifluoroacetate ligands adopt a bidentate coordination mode with silver atoms located in the top and bottom triangular planes, respectively, while the remaining four trifluoroacetate ligands also coordinate in a bidentate fashion, bridging one silver atom from the triangular planes and another from the hexagonal plane connected by Py_2S ligands (Fig. S5). This coordination leads to a slight distortion of the cuboctahedral geometry.

2D Ag_{12}-bpm crystallizes in the trigonal $P\bar{3}$ space group (Table S2). The structure of its Ag_{12} cluster building blocks (Fig. 3a) is similar to that of one-dimensional ones. The Ag–Ag bond lengths of **2D Ag_{12}-bpm** range from 3.004 to 3.199 Å, with an average of 3.069 Å, which is slightly shorter than those observed in **1D Ag_{12}-Py_2S** (3.141 Å). The Ag–S bond lengths range from 2.465 to 2.569 Å, averaging 2.506 Å. Interestingly, in contrast to the bidentate coordination mode of trifluoroacetate ligands observed in **1D Ag_{12}-Py_2S**, all six trifluoroacetate ligands in **2D Ag_{12}-bpm** are monodentately coordinated to silver atoms located on the top and bottom triangular planes (Fig. S6). The average Ag–O bond length in **2D Ag_{12}-bpm** is 2.446 Å, which is slightly longer than those observed in **1D Ag_{12}-Py_2S** (2.418 Å). Furthermore, in **2D Ag_{12}-bpm**, all six equatorial silver atoms on the hexagonal plane are coordinated by bpm linkers. As shown in Fig. 3a, the six bpm linkers attached to each Ag_{12} building blocks are individually connected to neighboring Ag_{12} units. Owing to the linear geometry of the bpm linker, the resulting assembly adopts a two-dimensional structure (Fig. 3b).

3D Ag_{12}-tmdp crystallizes in the trigonal $R\bar{3}c$ space group (Table S3). Single-crystal structure analysis reveals that, similar to **1D Ag_{12}-Py_2S** and **2D Ag_{12}-bpm**, the Ag_{12} cluster node in 3D Ag_{12}-tmdp retains a cuboctahedral geometry, with six thiolate ligands coordinated to the square face and six trifluoroacetate ligands monodentately coordinated on silver atoms located on the top and bottom triangular planes (Fig. 4a). The average Ag–Ag, Ag–S, and Ag–O bond lengths in **3D Ag_{12}-tmdp** are 3.101, 2.508 and 2.419 Å, respectively, closely resembling those observed in **1D Ag_{12}-Py_2S** (3.141, 2.504, and 2.418 Å) and **2D Ag_{12}-bpm** (3.069, 2.506 and 2.446 Å). In addition, each Ag_{12}

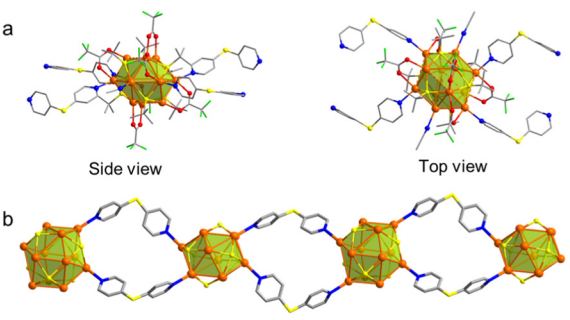

Fig. 2 (a) Side and top views of the Ag_{12} building block with four pendent Py_2S linkers in **1D Ag_{12}-Py_2S**. (b) Structure of **1D Ag_{12}-Py_2S**. Color legend: orange, Ag; yellow, S; red, O; green, F; blue, N; gray, C. All hydrogen atoms are omitted for clarity.

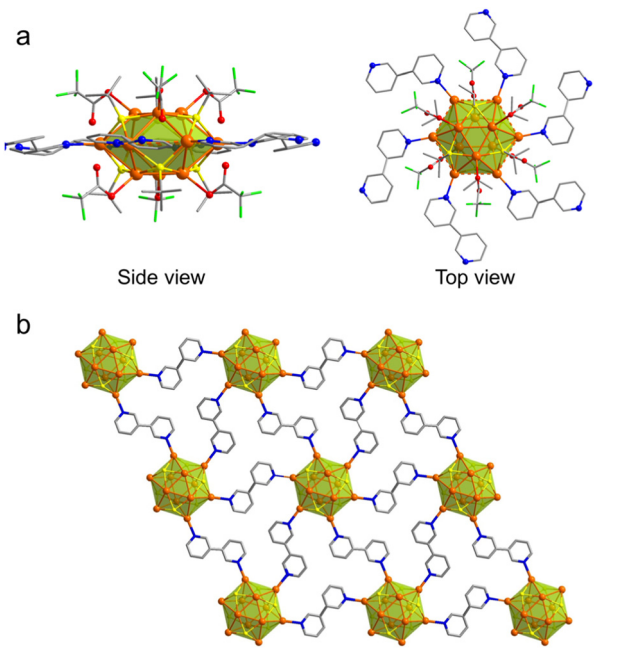

Fig. 3 (a) Side and top views of the Ag_{12} building block with six pendent bpm linkers in **2D Ag_{12}-bpm**. (b) Structure of **2D Ag_{12}-bpm**. Color legend: orange, Ag; yellow, S; red, O; green, F; blue, N; gray, C. All hydrogen atoms are omitted for clarity.

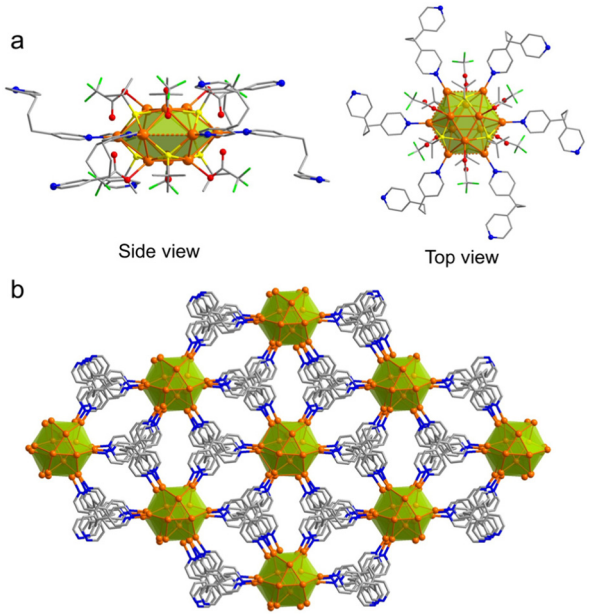

Fig. 4 (a) Side and top views of the Ag_{12} building block with six pendent tmdp linkers in **3D Ag_{12}-tmdp**. (b) Structure of **3D Ag_{12}-tmdp**. Color legend: orange, Ag; yellow, S; red, O; green, F; blue, N; gray, C. All hydrogen atoms are omitted for clarity.

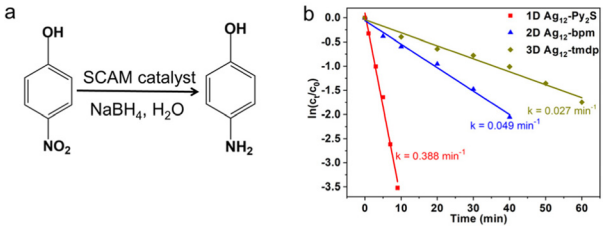

Fig. 5 Catalytic properties of **1D Ag_{12}-Py_2S**, **2D Ag_{12}-bpm** and **3D Ag_{12}-tmdp** SCAMs. (a) The reduction of 4-NP to 4-AP in the presence of SCAM catalyst. (b) Plot of $\ln(C_t/C_0)$ *versus* time for 1D–3D SCAMs.

core is interconnected by six bidentate tmdp ligands, which are arranged in a triangular planar pattern, forming an infinitely extending 3D honeycomb framework structure (Fig. 4b).

To verify the purity of the cluster-assembled crystals, powder X-ray diffraction (PXRD) data were collected for the powder samples. The PXRD patterns match well with the simulated patterns from single-crystal data, confirming the high purity of the crystals (Fig. S7–S9). As shown in Fig. S10, the UV-vis absorption spectra of the solid powders **1D Ag_{12}-Py_2S**, **2D Ag_{12}-bpm** and **3D Ag_{12}-tmdp** exhibit a similar declining trend without distinct absorption peaks. They all exhibit clear blue emission at ~442 nm with excitation at ~292 nm at room temperature (Fig. S11).

The three Ag_{12}-based SCAMs share the same Ag_{12} cluster as the common building unit, while their dimensionalities are systematically tuned to 1D, 2D, and 3D. This structural consistency, combined with controlled dimensional variation, provides a suitable platform for investigating how dimensionality influences catalytic performance. The catalytic hydrogenation of nitroaromatics to aminoaromatics, a reaction of both chemical and environmental significance, was chosen as a representative transformation.[45–47] Specifically, the reduction of 4-nitrophenol (4-NP) to 4-aminophenol (4-AP) using $NaBH_4$ served as the model reaction (Fig. 5a), with progress monitored by time-dependent UV-vis spectroscopy.[48–50] Upon introducing $NaBH_4$ into the 4-NP/SCAM mixture, the characteristic absorption peak of 4-NP at 400 nm gradually diminished, while a new peak at 300 nm corresponding to 4-AP emerged, confirming catalytic activity in all three systems (Fig. S12). Notably, the **1D Ag_{12}-Py_2S** material exhibited the highest catalytic efficiency, achieving complete conversion (Fig. S12d) within just 11 minutes (rate constant k = 0.388 min^{-1}, Fig. 5b). In comparison, the **2D Ag_{12}-bpm** and **3D Ag_{12}-tmdp** assemblies required 60 and 80 minutes, respectively (rate constants k = 0.049 and 0.027 min^{-1}, Fig. 5b), to reach full conversion (Fig. S12d). The PXRD patterns of SCAMs after catalysis are in good agreement with those of the as-synthesized materials (Fig. S13), indicating that the framework structures seem to be preserved under the reaction conditions.

The reduction of 4-NP by $NaBH_4$ is a typical surface-catalyzed reaction that follows a Langmuir–Hinshelwood mechanism, which has been well established.[50–53] In this process, $NaBH_4$ serves as the hydrogen and electron donor, while the metal catalyst provides surface active sites to mediate electron and hydrogen transfer between BH_4^- and 4-NP. Specifically, BH_4^- is first activated on the Ag surface to generate reactive surface hydrogen species. Meanwhile, 4-nitrophenol is adsorbed onto the Ag surface in its phenolate form. The nitro group is then stepwise reduced through nitroso and hydroxylamine intermediates to finally form 4-aminophenol. In this mechanism, the Ag_{12}-based SCAMs mainly function as heterogeneous catalysts by providing accessible Ag active sites and facilitating interfacial electron/hydrogen transfer. Kinetic studies show that the plots of $\ln(C_t/C_0)$ *versus* reaction time display good linearity (Fig. 5b), indicating that the reaction follows first-order kinetics with respect to 4-NP under excess $NaBH_4$ conditions. This kinetic behavior suggests that the concentration of BH_4^- remains effectively constant during the reaction, and the overall reaction rate is mainly governed by the reduction of adsorbed 4-NP.

Given that the three assembled materials are constructed from the same Ag_{12} cluster as the common building unit, the observed differences in catalytic activity can be reasonably correlated with variations in the surface accessibility of the Ag atoms. Structural analysis (Fig. S14), together with the van der Waals (vdW) surface area calculations (Table S4), demonstrates that the 1D architecture possesses the highest fraction of exposed Ag surface, followed by the 2D structure, while the 3D framework exhibits the lowest accessibility. The relative percentage of exposed Ag surface follows the order 1D > 2D > 3D, which aligns with the experimentally observed catalytic activity trend. This correlation suggests that a higher degree of Ag surface exposure is beneficial for providing more available

active sites and facilitating interfacial electron and hydrogen transfer during the reaction. It should be noted, however, that surface accessibility is regarded as one of the contributing factors, rather than the sole determinant, governing the catalytic differences among the three SCAMs, as other factors such as mass transport and microenvironment effects may also play a role. These findings clearly demonstrate that cluster dimensionality plays a certain role in modulating catalytic properties by shaping the structural and physicochemical environment of the active sites, offering a promising strategy for the rational design of high-performance nanocluster-based catalysts.

4 Conclusions

This work presents a strategic approach to linker design for assembling identical Ag_{12} NCs into 1D, 2D, and 3D frameworks, preserving the core intact across all architectures. Through directional N-donor ligands of varying lengths, the study achieves precise cluster assembly in all the dimensions, forming Ag cluster assembled structures with covalently connected cuboctahedral nodes. Single-crystal X-ray diffraction confirms structural integrity, enabling direct inference of how dimensionality influences function. Notably, the **1D Ag_{12}-Py_2S** framework demonstrates superior catalytic activity in the hydrogenation of nitroaromatics to aminoaromatics, attributed to rational catalysis in 1D assembly due to accessible active sites. These findings highlight the critical role of framework dimensionality in tuning material properties and mark a long vision toward designing atomically precise nanomaterials. This rational strategy paves the way for advanced applications in catalysis and nanotechnology.

Author contributions

X. L., G. D. and M. S. B. wrote the manuscript. X. L. and T. K. conceived and carried out experiments. X. L. and S. Y. conducted the characterization studies. G. D. and T. H. supervised the project.

Conflicts of interest

There are no conflicts to declare.

Data availability

The data supporting this article have been included as part of the supplementary information (SI). Supplementary information is available. See DOI: https://doi.org/10.1039/d5nr04708k.

CCDC 2450210, 2450211 and 2450418 contain the supplementary crystallographic data for this paper.[54a–c]

Acknowledgements

T. H. acknowledges the financial support by the Research Center Program of the IBS (IBS-R006-D1) in Korea. M. S. B. acknowledges the IBS for the Young Scientist Fellowship (IBS-R006-Y2).

References

1 M. A. Boles, M. Engel and D. V. Talapin, *Chem. Rev.*, 2016, **116**, 11220–11289.
2 R. Jin, C. Zeng, M. Zhou and Y. Chen, *Chem. Rev.*, 2016, **116**, 10346–10413.
3 M. Li, H. Schnablegger and S. Mann, *Nature*, 1999, **402**, 393–395.
4 B. Zhang, M. F. Matus, Q. Yao, X. Song, Z. Wu, W. Hu, H. Häkkinen and J. Xie, *J. Am. Chem. Soc.*, 2025, **147**, 6404–6414.
5 C. P. Joshi, M. S. Bootharaju, M. J. Alhilaly and O. M. Bakr, *J. Am. Chem. Soc.*, 2015, **137**, 11578–11581.
6 C. Zhao, Z. Zhang, F. Han, D. Xia, C. Xiao, J. Fang, Y. Zhang, B. Wu, S. You, Y. Wu and W. Li, *Angew. Chem., Int. Ed.*, 2021, **60**, 8526–8531.
7 X. Ji, Q. Li, H. Song and C. Fan, *Adv. Mater.*, 2022, **34**, 2201562.
8 I. Chakraborty and T. Pradeep, *Chem. Rev.*, 2017, **117**, 8208–8271.
9 N. Xia, J. Yang and Z. Wu, *Nanoscale*, 2015, **7**, 10013–10020.
10 Y. Du, H. Sheng, D. Astruc and M. Zhu, *Chem. Rev.*, 2020, **120**, 526–622.
11 M. Yang, H. Chan, G. Zhao, J. H. Bahng, P. Zhang, P. Král and N. A. Kotov, *Nat. Chem.*, 2017, **9**, 287–294.
12 S. E. Lohse and C. J. Murphy, *J. Am. Chem. Soc.*, 2012, **134**, 15607–15620.
13 Q. Li, J. C. Russell, T.-Y. Luo, X. Roy, N. L. Rosi, Y. Zhu and R. Jin, *Nat. Commun.*, 2018, **9**, 3871.
14 H. Zhao, C. Zhang, B. Han, Z. Wang, Y. Liu, Q. Xue, C.-H. Tun and D. Sun, *Nat. Synth.*, 2024, **3**, 517–526.
15 F. Hu, G. Yang, Z.-C. Long, W.-Q. Shi, G.-J. Liang, J.-Q. Wang and Q.-M. Wang, *Small*, 2025, **21**, 2502106.
16 A. Zada, P. Muhammad, W. Ahmad, Z. Hussain, S. Ali, M. Khan, Q. Khan and M. Maqbool, *Adv. Funct. Mater.*, 2020, **30**, 1906744.
17 R. Jin, G. Li, S. Sharma, Y. Li and X. Du, *Chem. Rev.*, 2021, **121**, 567–648.
18 G. Deng, H. Yun, Y. Chen, S. Yoo, K. Lee, J. Jang, X. Liu, C. W. Lee, Q. Tang, M. S. Bootharaju, Y. J. Hwang and T. Hyeon, *Angew. Chem., Int. Ed.*, 2025, **64**, e202418264.
19 C. Zhou, M. Wang, Q. Yao, Y. Zhou, C. Hou, J. Xia, Z. Wang, J. Chen and J. Xie, *Aggregate*, 2024, **5**, e401.
20 N. Alam, A. K. Das, P. Chandrashekar, P. Baidya and S. Mandal, *Nanoscale*, 2024, **16**, 10087–10107.
21 S. Yoo, S. Yoo, G. Deng, F. Sun, K. Lee, H. Jang, C. W. Lee, X. Liu, J. Jang, Q. Tang, Y. J. Hwang and T. Hyeon, *Adv. Mater.*, 2024, **36**, 2313032.

22 M. Cao, S. Wang, J.-H. Hu, B.-H. Lu, Q.-Y. Wang and S.-Q. Zang, *Adv. Sci.*, 2022, **9**, 2103721.
23 D. Zuo, H. Guo, Q. Xu, A. He, Z. Li, S. Li and H. Shen, *Nanoscale*, 2024, **16**, 20228–20234.
24 Y. Lu and W. Chen, *Chem. Soc. Rev.*, 2012, **41**, 3594–3623.
25 D. Yang, J. Wang, Q. Wang, Z. Yuan, Y. Dai, C. Zhou, X. Wan, Q. Zhang and Y. Yang, *ACS Nano*, 2022, **16**, 15681–15704.
26 H. Shen, G. Deng, S. Kaappa, T. Tan, Y.-Z. Han, S. Malola, S.-C. Lin, B. K. Teo, H. Häkkinen and N. Zheng, *Angew. Chem., Int. Ed.*, 2019, **58**, 17731–17735.
27 X. Liu, J. Chen, J. Yuan, Y. Li, J. Li, S. Zhou, C. Yao, L. Liao, S. Zhuang, Y. Zhao, H. Deng, J. Yang and Z. Wu, *Angew. Chem., Int. Ed.*, 2018, **57**, 11273–11277.
28 Y. Jin, C. Zhang, X. Y. Dong, S. Q. Zang and T. C. W. Mak, *Chem. Soc. Rev.*, 2021, **50**, 2297–2319.
29 Y. Li, X.-M. Luo, P. Luo, Q.-X. Zang, Z.-Y. Wang and S.-Q. Zang, *ACS Nano*, 2023, **17**, 5834–5841.
30 X. Liu, T. Ki, G. Deng, S. Yoo, K. Lee, B.-H. Lee, T. Hyeon and M. S. Bootharaju, *Nanoscale*, 2024, **16**, 12329–12344.
31 C. Zhang, W.-D. Si, Z. Wang, C.-H. Tung and D. Sun, *Angew. Chem., Int. Ed.*, 2024, **63**, e202404545.
32 Q. Yao, M. Zhu, Z. Yang, X. Song, X. Yuan, Z. Zhang, W. Hu and J. Xie, *Nat. Rev. Mater.*, 2025, **10**, 89–108.
33 J. Sakai, K. Sasaki, R. Nakatani, S. Das and Y. Negishi, *Nanoscale*, 2024, **16**, 21767–21775.
34 S. Biswas, S. Das and Y. Negishi, *Coord. Chem. Rev.*, 2023, **492**, 215255.
35 R. Nakatani, S. Biswas, T. Irie, J. Sakai, D. Hirayama, T. Kawawaki, Y. Niihori, S. Das and Y. Negishi, *Nanoscale*, 2023, **15**, 16299–16306.
36 X.-Y. Dong, Y. Si, J.-S. Yang, C. Zhang, Z. Han, P. Luo, Z.-Y. Wang, S.-Q. Zang and T. C. W. Mak, *Nat. Commun.*, 2020, **11**, 3678.
37 P. Chandrashekar, A. Karmakar, R. K. Aparna, L. Singh, P. K. Mondal, S. Kundu, K. Bhattacharyya and S. Mandal, *Chem. Sci.*, 2025, **16**, 5726–5734.
38 R.-W. Huang, Y.-S. Wei, X.-Y. Dong, X.-H. Wu, C.-X. Du, S.-Q. Zang and T. C. W. Mak, *Nat. Chem.*, 2017, **9**, 689–697.
39 G. Deng, B. K. Teo and N. Zheng, *J. Am. Chem. Soc.*, 2021, **143**, 10214–10220.
40 Z.-Y. Wang, M.-Q. Wang, Y.-L. Li, P. Luo, T.-T. Jia, R.-W. Huang, S.-Q. Zang and T. C. W. Mak, *J. Am. Chem. Soc.*, 2018, **140**, 1069–1076.
41 N. Alam, T. Rahaman, A. K. Das, A. K. Pal, A. Datta, S. J. Ray, P. K. Mondal, M. Polentarutti and S. Mandal, *Small*, 2025, **21**, 2409118.
42 M. J. Alhilaly, R.-W. Huang, R. Naphade, B. Alamer, M. N. Hedhili, A.-H. Emwas, P. Maity, J. Yin, A. Shkurenko, O. F. Mohammed, M. Eddaoudi and O. M. Bakr, *J. Am. Chem. Soc.*, 2019, **141**, 9585–9592.
43 W. A. Dar, A. Jana, K. S. Sugi, G. Paramasivam, M. Bodiuzzaman, E. Khatun, A. Som, A. Mahendranath, A. Chakraborty and T. Pradeep, *Chem. Mater.*, 2022, **34**, 4703–4711.
44 W. A. Dar, M. Bodiuzzaman, D. Ghosh, G. Paramasivam, E. Khatun, K. S. Sugi and T. Pradeep, *ACS Nano*, 2019, **13**, 13365–13373.
45 M. Qu, F.-Q. Zhang, G.-L. Zhang, M.-M. Qiao, L.-X. Zhao, S.-L. Li, M. Walter and X.-M. Zhang, *Angew. Chem.*, 2024, **136**, e202318390.
46 H. Zhou, T. Duan, Z. Lin, T. Yang, H. Deng, S. Jin, Y. Pei and M. Zhu, *Adv. Sci.*, 2024, **11**, 2307085.
47 L. Chen, F. Sun, Q. Shen, L. Qin, Y. Liu, L. Qiao, Q. Tang, L. Wang and Z. Tang, *Nano Res.*, 2022, **15**, 8908–8913.
48 Z. Wang, R. K. Gupta, F. Alkan, B.-L. Han, L. Feng, X.-Q. Huang, Z.-Y. Gao, C.-H. Tung and D. Sun, *J. Am. Chem. Soc.*, 2023, **145**, 19523–19532.
49 Z.-J. Guan, R.-L. He, S.-F. Yuan, J.-J. Li, F. Hu, C.-Y. Liu and Q.-M. Wang, *Angew. Chem., Int. Ed.*, 2022, **61**, e202116965.
50 S.-F. Yuan, Z.-J. Guan and Q.-M. Wang, *J. Am. Chem. Soc.*, 2022, **144**, 11405–11412.
51 S. M. Ansar and C. L. Kitchens, *ACS Catal.*, 2016, **6**, 5553–5560.
52 S. M. Ansar, F. S. Ameer, W. Hu, S. Zou, C. U. Pittman and D. Zhang, *Nano Lett.*, 2013, **13**, 1226–1229.
53 S. Wunder, Y. Lu, M. Albrecht and M. Ballauff, *ACS Catal.*, 2011, **1**, 908–916.
54 (*a*) CCDC 2450210: Experimental Crystal Structure Determination, 2026, DOI: 10.5517/ccdc.csd.cc2n7n1m; (*b*) CCDC 2450211: Experimental Crystal Structure Determination, 2026, DOI: 10.5517/ccdc.csd.cc2n7n2n; (*c*) CCDC 2450418: Experimental Crystal Structure Determination, 2026, DOI: 10.5517/ccdc.csd.cc2n7vrj.